THE JOURNAL OF PHYSICAL CHEMISTRY C

Article

pubs.acs.org/JPCC

Insights into the Structure of Dot@Rod and Dot@Octapod CdSe@CdS Heterostructures

Anna Corrias,*[,†] Erika Conca,[‡] Giannantonio Cibin,[§] Gavin Mountjoy,[†] Diego Gianolio,[§] Francesco De Donato,[∥] Liberato Manna,[∥] and Maria Francesca Casula*[,‡]

[†]School of Physical Sciences, Ingram Building, University of Kent, CT2 7NH, Canterbury, U.K.

[‡]Dipartimento di Scienze Chimiche e Geologiche and INSTM, Università di Cagliari, Cittadella Universitaria, I-09042 Monserrato (CA), Italy

[§]Diamond Light Source, Harwell Campus, Didcot, Oxon OX11 ODE, U.K.

[∥]Nanochemistry, Istituto Italiano di Tecnologia, I.I.T. Via Morego 30, I-16163 Genova, Italy

Supporting Information

ABSTRACT: CdSe@CdS dot@rods with diameter around 6 nm and length of either 20, 27, or 30 nm and dot@octapods with pod diameters of ∼15 nm and lengths of ∼50 nm were investigated by X-ray absorption spectroscopy. These heterostructures are prepared by seed-mediated routes, where the structure, composition, and morphology of the CdSe nanocrystals used as a seed play key roles in directing the growth of the second semiconducting domain. The local structural environment of all the elements in the CdSe@CdS heterostructures was investigated at the Cd, S, and Se K-edges by taking advantage of the selectivity of X-ray absorption spectroscopy, and was compared to pure reference compounds. We found that the structural features of dot@rods are independent of the size of the rods. These structures can be described as made of a CdSe dot and a CdS rod, both in the wurtzite phase with a high crystallinity of both the core and the rod. This result supports the effectiveness of high temperature colloidal synthesis in promoting the formation of core@shell nanocrystals with very low defectivity. On the other hand, data on the CdSe@CdS with octapod morphology suggest the occurrence of a core composed of a CdSe cubic sphalerite phase with eight pods made of CdS wurtzite phase. Our findings are compared to current models proposed for the design of functional heterostructures with controlled nanoarchitecture.

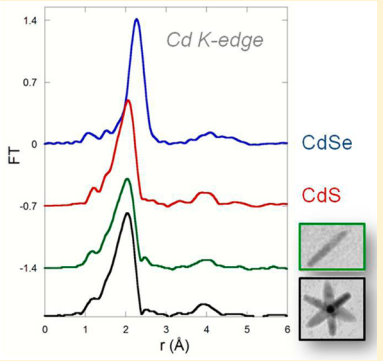

1. INTRODUCTION

Semiconductor chalchogenide nanocrystals, thanks to the very high degree of sophistication reached in controlled synthetic procedures, play a key role as model systems for the elucidation of crystal growth and assembly at the nanoscale.[1]

In particular, the development of protocols that are effective in achieving shape control has enabled the design of chalchogenides with tunable properties for targeted applications in fields as diverse as biosensing and photovoltaics. Among the proposed chalcogenide preparation routes, a major contribution has been provided by high temperature colloidal synthesis, where mastering of the synthetic parameters controlling polymorphism and relative energy of crystal facets, which both have a major role in directing nanocrystal shape, has been achieved.[2−5]

Because of the expected impact on energy and environment through the development of solar cell components and photocatalysts, intense efforts have been devoted to the preparation of hybrid chalcogenide heterostructures containing two or more chalcogenide nanostructured domains. In fact, by tuning the composition (hence band offsets alignment), size, shape, crystal phase, and crystallinity, and interconnection between the different chalcogenide domains, the optical and electronic properties of the resulting hybrid nanostructures can be optimized.

Among these hybrid nanostructures, CdSe@CdS nanorods made out of a cadmium selenide dot within a sulfide nanorod have attracted much attention due to the strong and tunable light emission combined with optimized visible light absorption.[6,7]

These heterostructures can be prepared through seed-mediated colloidal approaches which make use of a CdSe dot in the wurtzite hexagonal polymorph as a seed for the growth of CdS in the same wurtzite polymorph, mediated by a mixture of hot surfactants suited for directing anisotropic growth, as depicted in Figure 1a. Experimental and computational investigation of CdSe@CdS rods has enabled further insights into the correlations among the morphological and structural features of the dot@rods and quantum confinement of charge carriers, surface boundaries effects, and electron−hole recombination dynamics.[8] One key issue was whether the

Received: March 20, 2015
Revised: June 9, 2015
Published: June 25, 2015

DOI: 10.1021/acs.jpcc.5b04593
J. Phys. Chem. C 2015, 119, 16338−16348

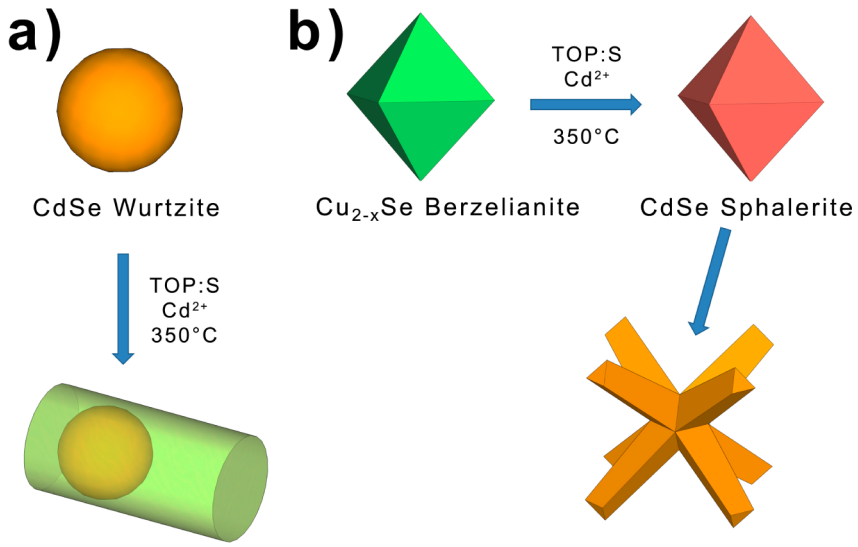

Figure 1. Schematic representation of the model proposed for the seeded growth of anisotropic chalcogenide heterostructures: CdSe@CdS rods (a) and octapods (b).

structure of the original CdSe seed was preserved in the final CdSe@CdS dot@rod structure.

More recently, advances in the seed-mediated colloidal method has led to the development of CdSe@CdS octapods made of eight arms of cadmium sulfide in the wurtzite polymorph departing from a central CdSe core. As opposed to the dot@rods, the synthesis of the dot@octapods is less straightforward and includes the synthesis of $Cu_{2-x}Se$ nanocrystals in the cubic berzelianite phase, their conversion into CdSe nanocrystals in the sphalerite (zinc blende) polymorph by Cu/Cd cation exchange, and the use of the thus-obtained dots as seeds for the branched growth of eight CdS arms in the wurtzite form (see Figure 1b). While the three-dimensional shape of these architectures has been elucidated by advanced transmission electron microscopy (TEM) techniques such as electron tomography and image reconstruction, no conclusive information has been inferred so far on the state of the CdSe dot, being located at the core of the octapod structure.[9]

In addition, although chemical analysis and TEM at the different stages of the octapod synthesis provided evidence of fast and nearly quantitative Cu/Cd ion exchange, no information on the location of any residual copper ions could be obtained. It is noteworthy that conventional structural investigation techniques such as X-ray diffraction (XRD) cannot provide insights on these aspects due to the very large amount of CdS in the wurtzite phase which dominates the diffraction pattern accompanied by the broadening of the peaks due to small nanocrystal size, thus making the sensitivity of this technique for nanocrystals relatively poor.

An additional issue is related to the optical properties of CdSe@CdS octapod nanocrystals which are known as inefficient emitters, as opposed to other CdSe@CdS colloidal nanostructures, such as spherical core@shell dots and rods. The low photoluminescence quantum yield could have been tentatively ascribed either to electric potential barriers and crystal defects at the CdSe@CdS interface, inhibiting the relaxation of holes into the CdSe core, or to residual Cu as dopants in the octapod nanostructures, acting as traps. Intentional or unintentional ion doping, as well as the nature of the interface at different chalcogenide domains represent relevant issues in nanocrystal design, as they have been shown to deeply impact the photophysical properties of colloidal heterostructures and may overcome size and shape effects.[10,11]

In this work, we address the characterization of CdSe@CdS rods and octapods by exploiting the selectivity and sensitivity of X-ray absorption spectroscopy. X-ray absorption spectroscopy (AXS) techniques are very suitable methods for the detailed investigation of multicomponent materials because they are elemental specific and, hence, can examine separately the environment of every atom. In particular, quantitative structural information on the local structure of selected absorbing atoms in multicomponent materials can be obtained from the extended X-ray absorption fine structure (EXAFS) spectra and described in terms of number and type of neighboring atoms, interatomic distances, and Debye–Waller factors.[12] X-ray absorption near edge structure (XANES) can also provide additional information in terms of oxidation number and coordination geometry.[12]

EXAFS is a suitable structural tool as it may provide information also in the case of a very diluted concentration of the selected atom, allowing one in this particular case (i) to study the Se structural environment that would be hard to achieve with other techniques and (ii) to gather more detailed information on the effectiveness of the Cu/Cd ion exchange. Because EXAFS is a technique that probes the short-range order, it has been shown to be a very powerful tool for the study of nanomaterials, including core@shell nanostructures and chalcogenide-based heterostructures.[13−25] It should however be pointed out that EXAFS is a technique providing information on the bulk, and therefore it needs to be used in a complementary way to other characterization techniques which are able to look at individual nanoparticles. In the case of nearly monodisperse particles having a high degree of homogeneity in terms of shape and size, the collective features of the sample can be effectively correlated to the structure of the individual nanocrystals and therefore X-ray absorption spectroscopy is particularly suited for these kinds of materials.

Here, we carry out a multiedge (Cd, S, Se, and Cu K-edges) EXAFS study of chalcogenide heterostructures prepared through seed-mediated high-temperature colloidal routes. The samples are made of CdSe@CdS dot@rods with different lengths (in the range 20−30 nm) which were grown from

DOI: 10.1021/acs.jpcc.5b04593
J. Phys. Chem. C 2015, 119, 16338−16348

Table 1. Summary of the Nanocrystals, Reference Compounds, and Related Features[a]

sample	EXAFS sample	investigated edges	features
Rod 1	toluene suspension	Cd K-edge (T) S K-edge (TEY) Se K-edge (F)	dot size 4.9 nm rod length 21.5 ± 2.6 nm rod diameter 6.0 ± 0.6 nm
Rod 2	toluene suspension	Cd K-edge (T) S K-edge (TEY) Se K-edge (F)	dot size 4.9 nm rod length 27.7 ± 8.7 nm rod diameter 5.6 ± 0.6 nm
Rod 3	toluene suspension	Cd K-edge (T) S K-edge (TEY) Se K-edge (F)	dot size 4.9 nm rod length 30.1 ± 3.9 nm rod diameter 6.0 ± 0.6 nm
Octa	toluene suspension	Cd K-edge (T) S K-edge (TEY) Se K-edge (F) Cu K-edge (F,T)	dot size 15 nm arm length 50.0 ± 2.2 nm arm width 14.9 ± 1.8 nm
CdS	commercial powder	Cd K-edge (T) S K-edge (F)	wurtzite polymorph
CdSe	commercial powder	Cd K-edge (T) Se K-edge (T)	wurtzite polymorph
CuCl	commercial powder	Cu K-edge (T)	sphalerite polymorph

[a]The EXAFS edges investigated in the detection mode (T = transmission; TEY = total electron yield; F = fluorescence) are also given.

nearly monodisperse ~5 nm CdSe wurtzite seed, and CdSe@CdS dot@octapods with pod length and width of 50 and 15 nm, respectively, starting from $Cu_{2-x}Se$ nanocrystals with sizes around 15 nm. Comparison of the structural environments of each selected atom in the different CdSe@CdS heterostructures and in pure commercial CdS, CdSe, and CuCl reference compounds provides evidence on the structure of the chalcogenide domains, on the degree of crystallinity, and on the occurrence of impurities. Our findings, corroborated by XANES data, provide experimental support for the models on the growth of shape-controlled chalcogenide heterostructures.

2. EXPERIMENTAL SECTION

Reference Materials. Cadmium sulfide in the hexagonal wurtzite polymorph (CdS, Aldrich 217921 powder, 99.995% trace metals basis), cadmium selenide in the wurtzite polymorph (CdSe, Alfa Aesar 45456, 99.999% trace metals basis), and cubic copper(I) chloride in the sphalerite polymorph (CuCl, Alfa Aesar 14644, 99.999% trace metals basis) were used as reference materials without further purification.

Synthesis of the CdSe@CdS Anisotropic Nanocrystals. CdSe@CdS dot-rods with different rod length (hereafter labeled samples Rod 1, Rod 2, and Rod 3) were prepared according to the protocol detailed in ref 4. Briefly, the CdSe seeds were first prepared by mixing under inert atmosphere in a three-neck flask tri-*n*-trioctylphosphine oxide (TOPO, 99%, Strem Chemicals, 3.0 g), octadecylphosphonic acid (ODPA, 99%, Polycarbon Industries, 0.280 g), and cadmium oxide (CdO, 99.999%, Strem Chemicals, 0.060 g). The mixture was heated up to 380 °C until complete dissolution of CdO. First tri-*n*-octylphosphine (TOP, 97%, Strem Chemicals, 0.5 g) and then a solution of TOP/Se (0.360 g TOP + 0.058 g Se, 99,99%, Strem Chemicals) were injected into the flask and left to react for 1 min, after which the reaction mixture was rapidly quenched. The so-obtained CdSe nanocrystals, having an average size of 4.8 nm, were isolated and purified by three cycles of precipitation though methanol (anhydrous, Carlo Erba), centrifugation, and dispersion in toluene (anhydrous, Carlo Erba). Finally, a suspension of the CdSe dots to be used as seeds for the growth of CdSe@CdS rods was prepared by dispersion in TOP and mixed with a solution of sulfur precursor (prepared by mixing 60 mg of S in 1.5 g of TOP). Such solution was then injected into a mixture of CdO (0.060 g), TOPO (3.0 g), ODPA (0.290 g), and *n*-hexylphosphonic acid (HPA, 99%, Polycarbon Industries, 0.080 g) previously heated in a three-neck flask under nitrogen atmosphere at 350 °C. After heating for 7 min, the flask was rapidly quenched and the dot@rods were purified by three repeated cycles of precipitation through the addition of methanol and centrifugation, followed by redispersion in toluene. By varying the amount of injected CdSe seeds from 2.8×10^{-2} to 2.1×10^{-2} and 1.4 × 10−2 μmol, Rod 1, Rod 2, and Rod 3 samples were obtained, respectively, which exhibited increasing rod length, as detailed in Table 1.

CdSe@CdS dot-octapods (hereafter labeled sample Octa) were prepared according to a recently developed protocol based on the anisotropic growth of CdS arms on CdSe seeds obtained from $Cu_{2-x}Se$ seeds by cation exchange.[26,27] Briefly, $Cu_{2-x}Se$ seeds were synthesized by reaction at 300 °C under inert atmosphere between a solution of CuCl (99.999%, Strem Chemicals) and oleylamine (70%, OLA, Sigma-Aldrich) in 1-octadecene (90%, Sigma-Aldrich) and a Se precursor solution prepared by dissolving Se in oleylamine. The resulting $Cu_{2-x}Se$ nanocrystals were purified and dispersed in TOP. To promote CdSe@CdS octapod formation, $Cu_{2-x}Se$ nanocrystals in TOP were mixed with a suspension of S in TOP and injected at 380 °C in a mixture containing CdO (99.99%, Sigma-Aldrich), $CdCl_2$ (99.99%, Sigma-Aldrich), ODPA, HPA, TOPO, and TOP. After the injection, the reaction was run for 10 min and then the solution was cooled to room temperature. The resulting product was purified by repeated washings with toluene and methanol and dispersed in toluene.

Sample Characterization. Transmission electron microscopy (TEM) images were recorded on a Hitachi H-7000 instrument using a thermoionic W gun at 125 kV, and equipped with a AMT DVC (2048 × 2048 pixel) CCD Camera. Prior to observation, a drop of the toluene-based suspension of the CdSe@CdS nanocrystals was deposited and dried at room temperature on a carbon-coated copper grid. Statistical analysis of TEM images by the freeware ImageJ software (ImageJ 1.42, Wayne Rasband, National Institute of Health, <http://rsb.info.nih.gov/ij/> (Java 1.6.0_14, 32 bit) was carried out in order to obtain size distribution plots from around 150 particles.

X-ray Diffraction (XRD) patterns were recorded on a Panalytical Empyrean diffractometer using Cu Kα radiation. The scans were collected in the 10°−90° (2θ) range in Bragg−Brentano geometry with a graphite monochromator on the diffracted beam and an X'Celerator linear detector. Prior to measurements, the nanocrystals were deposited from the toluene suspension on a low-background silicon sample holder. To avoid preferred orientation effects, the sample holder was spun at a rate of 1 Hz. Phase identification was performed using the PDF-2 database (PDF-2 JCPDS International Centre for Diffraction Data, Swarthmore, PA). The average size of crystallite domains was calculated using the Scherrer formula,

DOI: 10.1021/acs.jpcc.5b04593
J. Phys. Chem. C 2015, 119, 16338−16348

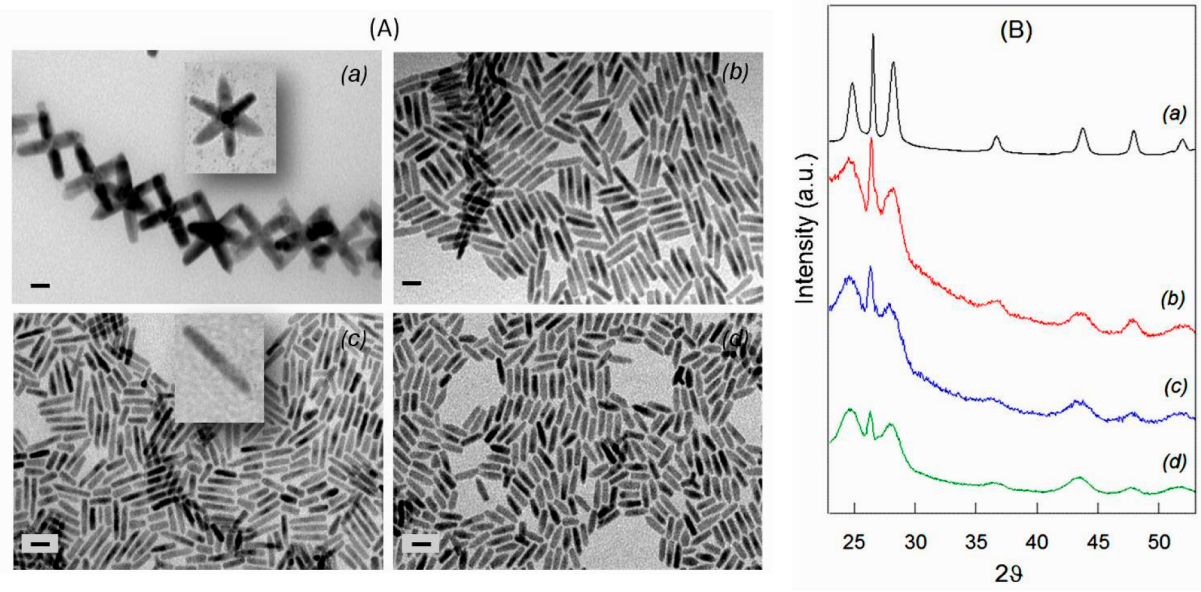

Figure 2. Transmission electron microscopy images (A) and X-ray diffraction patterns (B) of CdSe@CdS (d) Rod 1, (c) Rod 2, (b) Rod 3, and (a) Octa samples. Scale bar for all TEM images is 20 nm.

with instrumental broadening determined using a LaB_6 standard sample.[28]

X-ray Absorption Spectroscopy Measurements and Data Analysis. EXAFS spectra at room temperature were collected on Rod 1, Rod 2, Rod 3 and Octa samples and on CdS, CdSe, and CuCl reference compounds at the B18 beamline of the DIAMOND light source (Oxfordshire, UK), which covers a wide energy range (2.05 to 35 keV) and is equipped with a double-crystal monochromator containing two pairs of crystals, Si(111) and Si(311), optimized for quick EXAFS (QEXAFS) measurements.[29]

Spectra were acquired at the S (2472 eV), Cu (8979 eV), Cd (26711 eV), and Se (12658 eV) K-edges. The Si 111 monochromator was used for the S, Cu, and Se K-edges, and the Si 311 monochromator was used for the Cd K-edge.

At the S K-edge, data collection was performed under vacuum because of the low energy of the X-rays, using two different detectors: a fluorescence detector (for the CdS standard compound), and a total electron yield (TEY) detector (for all the samples). Samples were deposited from the toluene dispersion either on aluminum foil or on carbon sticky tape and dried.

At the Cu K-edge data were collected on the CuCl standard compound in transmission mode and on the Octa sample both in transmission and fluorescence mode.

At the Cd K-edge data on samples and standard compounds were all collected in transmission mode. The CdS and CdSe samples were measured as pellets made by mixing the standard compounds with polyvinylpyrrolidone, in order to have a highly uniform and suitable optical thickness, while the suspensions of the CdSe@CdS samples in toluene were measured using cells for liquids with kapton windows.

At the Se K-edge data were collected in transmission mode on the CdSe pellet and in fluorescence mode on the cells for liquids containing the suspensions of the CdSe@CdS in toluene.

The EXAFS data processing was carried out using the ATHENA software and the fit to scattering models in R-space was obtained by FEFF in Artemis.[30]

XANES spectra were also collected and the data processing was carried out using the ATHENA software to obtain normalized absorbance. The XANES results will be presented in the Supporting Information.

In Table 1 a list of the measured samples and acquisition conditions is summarized.

3. RESULTS AND DISCUSSION

3.1. X-ray Diffraction and Transmission Electron Microscopy. The Rod 1, Rod 2, Rod 3, and Octa nanostructures were investigated by conventional characterization techniques such as TEM and XRD to gain insights on the morphology and structure of the investigated samples. Figure 2A shows representative TEM images of the nanocrystals, which indicate the occurrence of nearly monodisperse rods with average width of 6 nm and length of 21.5, 27.7, and 30.0 nm, respectively, for the Rod 1, Rod 2, and Rod 3 samples, whereas the Octa sample exhibits octapod-shaped nanocrystals with average arm width of 15 nm and arm length of 30 nm. The results on the nanocrystal size distribution as obtained by statistical analysis of TEM images are summarized in Table 1. It is noteworthy that the CdSe core can be barely detected in the dot@rod nanocrystals as a slightly darker contrast close to one end of the rod, whereas the core at the center of the three-dimensional branched nanostructure octapods in the CdSe@CdS Octa sample cannot be imaged.

The XRD patterns for all the CdSe@CdS nanocrystals (Figure 2B) exhibit reflections which can be ascribed to the hexagonal (space group $P6_3mc$) CdS wurtzite polymorph (PDF card No. 41-1049], whereas the CdSe phase cannot be detected, likely due to the low relative contribution from the selenide domains with respect to the sulfide ones. In fact, diffraction peaks from the CdSe core have only been detected in patterns of CdSe@CdS core@shells with low aspect ratio or at early stages of sulfide growth from the selenide seed. As previously reported, the relative intensity and the line broadening of the peaks clearly reflect the anisotropic growth of the nanocrystals: in particular, the 002 reflection, centered at $2\theta \approx 26.5°$, is sharper and more intense in comparison to the

DOI: 10.1021/acs.jpcc.5b04593
J. Phys. Chem. C 2015, 119, 16338−16348

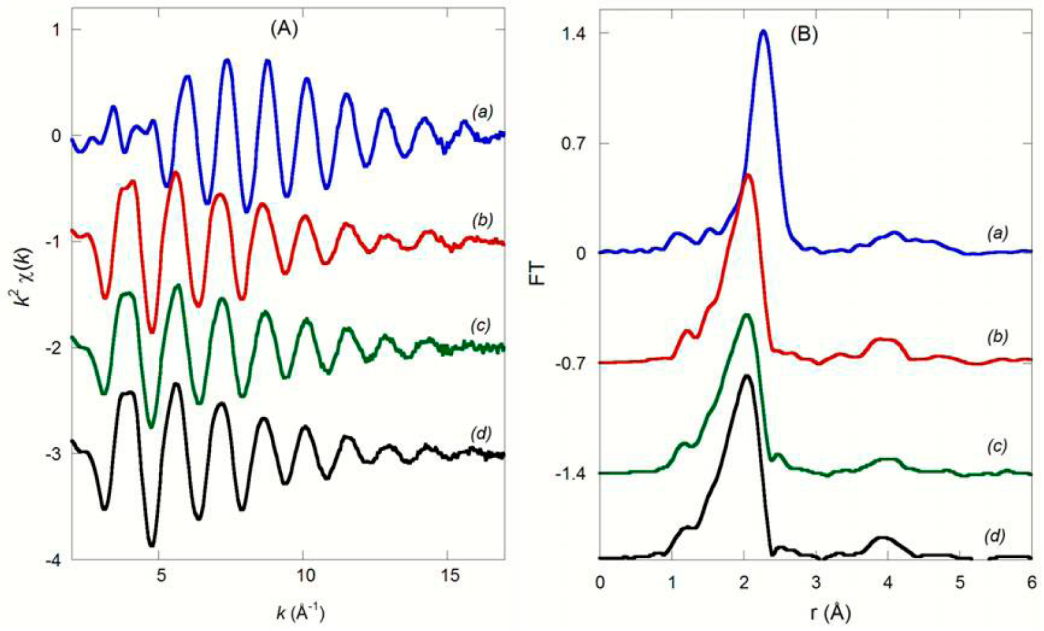

Figure 3. Experimental Cd K-edge $k^2\chi(k)$ (A) and corresponding FTs (B) for the CdSe (a) and CdS (b) reference compounds, and for the Rod 1 (c) and Octa (d) samples.

bulk wurtzite structure as a consequence of the nanocrystal growth along the *c* axis and its relative intensity increases in the order Rod 1, Rod 2, Rod 3, and Octa sample, as expected.[27,31]

3.2. X-ray Absorption Spectroscopy. *Cd K-Edge.* EXAFS data were collected to gather further insight on the structural environment in the CdSe dots and in the CdS rods/branches of the CdSe@CdS nanocrystals, in comparison with the bulk CdS and CdSe crystalline phases. Figure 3 shows the Cd K-edge $k^2\chi(k)$ and the corresponding Fourier transforms (FTs) for the Rod 1 and Octa samples. A qualitative comparison of the EXAFS results is first done in order to find an appropriate model to be chosen for the fitting that can provide quantitative structural parameters. In Table 2 the interatomic distances and coordination numbers for the shells up to 4.5 Å of the bulk CdS wurtzite polymorph and for the bulk wurtzite and sphalerite CdSe polymorphs are reported, as they are the phases which are the most likely present.

Table 2. Interatomic Distances (R) and Coordination Numbers (N) for Bulk CdS (Wurtzite Polymorph) and Bulk CdSe (Wurtzite and Sphalerite Polymorphs)

	Cd K-edge	
	R (Å)	N (Atoms)
	Bulk Wurtzite CdS	
S	2.526	3
S	2.532	1
Cd	4.119	6
Cd	4.136	6
	Bulk Wurtzite CdSe	
Se	2.628	3
Se	2.640	1
Cd	4.295	6
Cd	4.299	6
	Bulk Sphalerite CdSe	
Se	2.631	4
Cd	4.297	12

In Figure 3 Cd K-edge $k^2\chi(k)$ results of Rod 1 are compared with that of the Octa sample and also with the CdS and CdSe reference compounds: note that both reference compounds are in the wurtzite polymorph due to poor stability of the cubic sphalerite phase belonging to space group $F43m$.

For the sake of clarity only the EXAFS results of the Rod 1 sample are reported, because all the EXAFS results on the Rod 2 sample are identical within the experimental error to those of the Rod 1 sample, as shown in Figure S1, while the data of the Rod 3 sample are much noisier than those of Rod 1 and Rod 2 because the available toluene dispersion was much more diluted than in the other two samples. Since Rod 3 only differs very slightly in the dot and rod size compared to Rod 2, the data collected on Rod 3 will not be shown; it should be pointed out that even if data analysis was made more difficult due to the very low concentration of the Rod 3 sample, the data appear to be still comparable to the other two samples. Therefore, the structural features of Rod 1 can describe those of all the CdSe@CdS heterostructures grown in the form of rods with no influence coming from the length of the rods.

The data of both Rod 1 and Octa samples show a very close resemblance to the pure CdS, in agreement with the main component being CdS in the wurtzite structure both in the rods and in the octapods. On the other hand, the Cd K-edge $k^2\chi(k)$ of the pure CdSe reference compound shows some relevant differences: (i) the frequency of the oscillations is different and a shift is evident in the k region 5−18 Å^{-1}, in agreement with the larger interatomic distances in the Cd−Se unit cell as compared to those in the Cd−S unit cell (see Table 2) and to the different backscatterer in the first shell; and (ii) the amplitudes are different, especially in the k region 3−5 Å^{-1}. A closer inspection at the amplitudes and features of the oscillations in the rod, octa, and pure CdS confirms that the $k^2\chi(k)$ for the rods and octapods are quite similar to the CdS reference compound, and in particular the amplitudes of the

DOI: 10.1021/acs.jpcc.5b04593
J. Phys. Chem. C 2015, 119, 16338−16348

Table 3. Interatomic Distances (R), Coordination Numbers (N), and Debye-Waller Factors (σ) As Obtained from Best Fitting Parameters of the Experimental EXAFS Functions at the Cd, Se, and S K-Edges

Cd K-edge						
	Rod 1			Octa		
	R (Å)	N (Atoms)	$2\sigma^2$ (Å^2)	R (Å)	N (Atoms)	$2\sigma^2$ (Å^2)
S	2.504 ± 0.007	3	0.0060 ± 0.0006	2.517 ± 0.006	3	0.0043 ± 0.0005
S	2.509 ± 0.007	1	0.0060 ± 0.0006	2.522 ± 0.006	1	0.0043 ± 0.0005
Cd	4.08 ± 0.06	6	0.05 ± 0.01	4.14 ± 0.04	6	0.032 ± 0.008
Cd	4.09 ± 0.06	6	0.05 ± 0.01	4.16 ± 0.04	6	0.032 ± 0.008
		E_0 = 0.8 ± 0.5			E_0 = 2.4 ± 0.5	
		S_0 = 0.831			S_0 = 0.831	
		R-factor = 0.04054			R-factor = 0.0242	
Se K-edge						
sphalerite structure						
				Octa		
				R (Å)	N (Atoms)	$2\sigma^2$ (Å^2)
Cd				2.601 ± 0.005	4	0.0041 ± 0.0004
Se				4.33 ± 0.05	12	0.023 ± 0.009
					E_0 = 0.8 ± 0.4	
					S_0 = 0.76	
					R-factor = 0.04201	
wurtzite structure						
	Rod 1			Octa		
	R (Å)	N (Atoms)	$2\sigma^2$ (Å^2)	R (Å)	N (Atoms)	$2\sigma^2$ (Å^2)
Cd	2. 600 ± 0.005	3	0.0046 ± 0.0004	2.597 ± 0.004	3	0.0042 ± 0.0004
Cd	2.612 ± 0.005	1	0.0046 ± 0.0004	2.610 ± 0.004	1	0.0042 ± 0.0004
Se	4.32 ± 0.07	6	0.03 ± 0.01	4.32 ± 0.05	6	0.023 ± 0.009
Se	4.32 ± 0.07	6	0.03 ± 0.01	4.33 ± 0.05	6	0.023 ± 0.009
		E_0 = 0.8 ± 0.4			E_0 = 0.7 ± 0.4	
		S_0 = 0.76			S_0 = 0.76	
		R-factor =0.03761			R-factor =0.04507	
S K-edge						
	Rod 1			Octa		
	R (Å)	N (Atoms)	$2\sigma^2$ (Å^2)	R (Å)	N (Atoms)	$2\sigma^2$ (Å^2)
Cd	2.516 ± 0.009	3	0.0056 ± 0.0009	2.516 ± 0.007	3	0.0053 ± 0.0007
Cd	2.522 ± 0.009	1	0.0056 ± 0.0009	2.522 ± 0.007	1	0.0053 ± 0.0007
S	4.06 ± 0.03	6	0.022 ± 0.005	4.06 ± 0.02	6	0.018 ± 0.003
S	4.08 ± 0.03	6	0.022 ± 0.005	4.07 ± 0.02	6	0.018 ± 0.003
		E_0 = 3.3 ± 0.6			E_0 = 2.6 ± 0.5	
		S_0 = 0.821			S_0 = 0.821	
		R-factor =0.06633			R-factor =0.04146	

oscillations of the octapod in most of the k range are more similar to the pure CdS wurtzite sample than those of the rods. The comparison of the Fourier transforms of the Rod 1, Octa, pure CdS, and pure CdSe at the Cd K-edge, reported in Figure 3B, is in agreement with the discussion reported above. In particular, the samples exhibit well-defined peaks which reflect a highly structured environment and are both quite close to the FT of the pure CdS. The FT of the Octa sample exhibits a closer resemblance to pure CdS with respect to the rod samples.

The Cd K-edge XANES spectra of the Rod 1, Octa, pure CdS, and pure CdSe reported in Figure S2 show that Rod 1 and Octa samples have extremely similar XANES spectra to that for bulk CdS (wurtzite), confirming that Cd is tetrahedrally coordinated to S. There is no evidence for any contribution from CdSe. A significant contribution from CdSe would be noticeable because Figure S2 shows that the XANES spectrum for CdSe is clearly different to that for CdS.

The overall comparison of all the $k^2\chi(k)$, FTs, and XANES spectra obtained at the Cd K-edge, which suggests that distances, coordination numbers, and Debye−Waller factors in the nanocrystals are very similar to those of the pure wurtzite CdS polymorph, was used as a basis for the quantitative analysis of the data as obtained by fitting of the EXAFS data at the Cd K-edge.

In particular, the fit of the Octa, Rod 1, and Rod 2 data was done using the Cd−S paths (two paths with degeneracy 3 and 1, respectively) and Cd−Cd paths (two paths both with degeneracy 6) calculated on the basis of the hexagonal wurtzite polymorph. Since the fit results on Rod 2 are almost coincident with those of Rod 1, they are not presented for the sake of clarity. In Table 3 the best fitting parameters are reported while

DOI: 10.1021/acs.jpcc.5b04593
J. Phys. Chem. C 2015, 119, 16338−16348

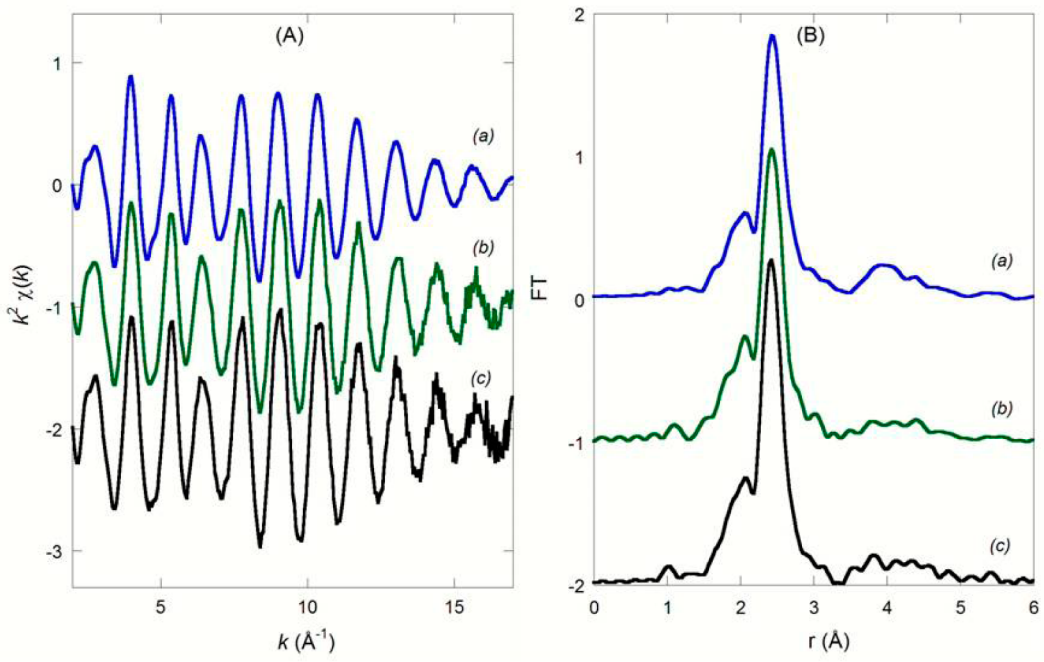

Figure 4. Experimental Se K-edge $k^2\chi(k)$ (A) and corresponding FTs (B) for the CdSe (a) reference compound, and for the Rod 1 (b) and Octa (c) samples.

the comparison of experimental vs fitting curves is reported in the Supporting Information (Figure S3 and S4).

The Cd−S and Cd−Cd interatomic distances are very close to those of pure CdS in the wurtzite polymorph, and the Debye−Waller factors are small confirming the high degree of order of the heterostructures. These results are consistent with the diameter and length of the rods and of the octapod arms, both being large enough that there is not a decrease in coordination numbers (which is expected only for particles smaller than 3 nm).[32] There is a small though significant difference in the E_0 best fit values obtained for the Octa and for the Rod 1 samples. It is likely that this is due to the different contribution from the CdSe core in the two samples that it is not taken into account in the fitting, in order to limit the number of free parameters.

It should be pointed out that the Debye−Waller factors for the nanocrystals are very similar to the bulk reference material. This is quite remarkable, since a significant increase in the Debye−Waller factors is generally observed in nanoparticles as a consequence of increased structural disorder, with particular reference to atoms located close to the surface. The obtained results indicate therefore a high degree of order of the whole heterostructures, including their surfaces. The high degree of crystallinity of the core@shell rods and octapods is a major advantage to be ascribed to the adopted synthetic route, based on colloidal growth at high temperature.

A closer inspection of Figure 3A showing the Cd K-edge $k^2\chi(k)$ of Rod 1 and Octa samples in the region 3−5 Å^{-1} provides some further insight on the effect of the CdSe core size and the relative CdSe/CdS amount since, as discussed previously, the differences between the CdS and CdSe reference compounds are stronger in that region. At around k = 4 Å^{-1} the Rod 1 sample exhibits slight differences with respect to the pure wurtzite CdS sample in the amplitudes of the oscillations and in some small features; these could be attributed to different effects such as the contribution of the Cd−Se distances arising from the CdSe dot and/or to the effect of the directional growth of the rod. Because the diameter and length of the rods are large enough that there is not a decrease of coordination numbers, it is very likely that the former effect is dominant. Likewise, in the region 3.6−4.1 Å^{-1} the features of the Octa sample are slightly different from both the pure CdS reference compound and the rod samples. These differences are likely due to the relative CdSe/CdS amount, which is smaller in the Octa than in the Rod 1 sample due to the size of the core and the length of the rod/pods together with number of pods. This observation is corroborated by Supporting Information, Figure S5, in which the difference between the $k^2\chi(k)$ of CdSe and CdS is compared with the difference between the $k^2\chi(k)$ of the Rod 1 sample and CdS, and the difference between the $k^2\chi(k)$ of the Octa sample and CdS. This comparison confirms that the Octa sample is more similar to CdS than the Rod 1 sample, and that this result can be ascribed to the Rod 1 sample having a larger fraction of CdSe contributing to the total $k^2\chi(k)$.

Hence, the influence of the Cd−Se distances should play an important role in determining the observed octapod function, possibly indicating a slightly different Cd−Se environment in the octapod sample compared to the rods.

Se K-Edge. The EXAFS spectra of the rod and octapod samples, together with the CdSe reference compound, were also collected at the Se K-edge. The Se K-edge $k^2\chi(k)$ and the corresponding Fourier transforms (FTs) for the Rod 1 and Octa samples and for the CdSe reference compound are reported in Figure 4, whereas data on the Rod 2, which are very similar to the Rod 1 sample, as already observed at the Cd K-edge, are shown as Supporting Information (Figure S6). Qualitative examination of the data, which was used to set up the quantitative analysis, indicates that the Se K-edge $k^2\chi(k)$ functions for the Rod 1 and Octa samples show strong oscillations up to high k values at exactly the same frequencies, and that the amplitude of the oscillations is higher in the Octa sample. This significant difference indicates a less disordered

DOI: 10.1021/acs.jpcc.5b04593
J. Phys. Chem. C 2015, 119, 16338−16348

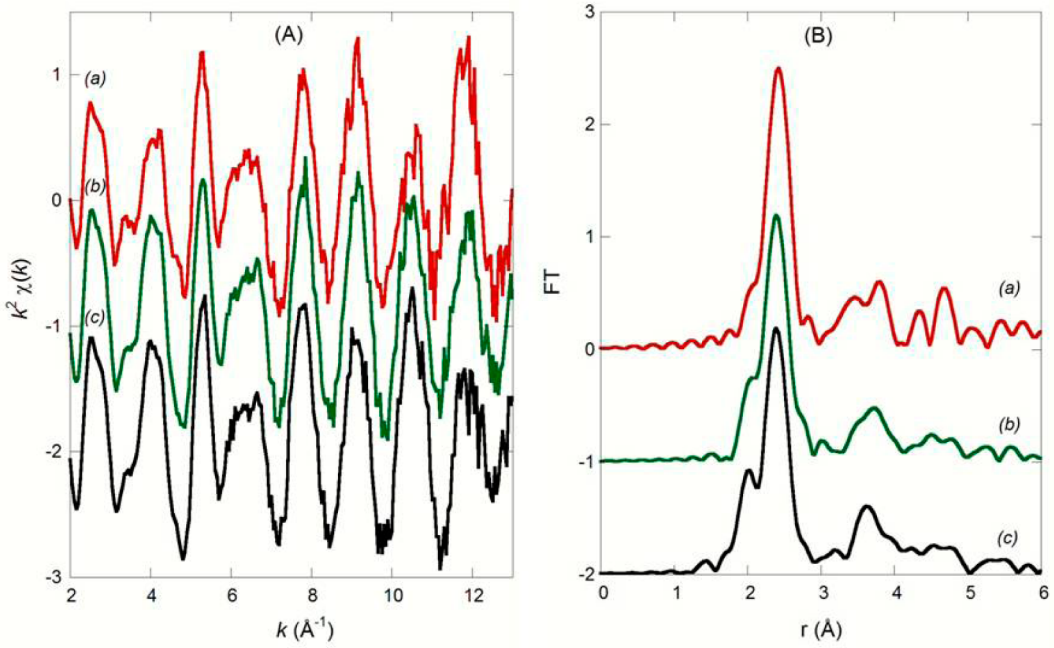

Figure 5. Experimental S K-edge $k^2\chi(k)$ (A) and corresponding FTs (B) for the CdS (a) reference compound, and for the Rod 1 (b) and Octa (c) samples.

environment in the octapod sample with respect to the rods samples. It should be noted that the samples could only be compared to the CdSe wurtzite polymorph, as the CdSe in the sphalerite phase is not commercially available, being poorly stable.

The comparison of the rod with the pure wurtzite CdSe sample shows some small differences both in the frequency (at k values the oscillations are slightly shifted) and in the amplitude (which is slightly larger for the rod samples) of the oscillations. These results suggest the occurrence of some differences in the Se environment in the CdSe dot at the interface with the CdS rod, as opposed to the pure CdSe sample. The Octa sample shows oscillations which have exactly the same frequency of the rod samples (no shift is detectable) and a more enhanced amplitude of the oscillations with respect to the pure wurtzite CdSe. In addition to differences in the Se environment at the interface between the dot and the arms, a less disordered environment can be therefore assumed in the CdSe core of the octapod sample with respect to the pure CdSe wurtzite. Although EXAFS data of the CdSe sphalerite polymorph are not available, it should be pointed out that the main difference between the cubic sphalerite and the hexagonal wurzite structures is that all the Se−Cd and Se−Se distances are exactly the same (as well as Cd−Cd distances which are not contributing to the Se K-edge structural function) in the cubic polymorph, whereas in the hexagonal polymorph there are two sets of Se−Cd and Se−Se distances, although very similar to each other (see Table 2). As a result, the sphalerite structure is slightly more ordered than the wurtzite structure. Therefore, the observed results suggest that the Se environment in the Octa sample is consistent with the more ordered structure of the sphalerite polymorph.

These results are also confirmed by the corresponding Fourier transforms (FTs) at the Se K-edge for the same samples, which are reported in Figure 4B. The FT of pure CdSe wurtzite shows the main peak at R values around 2.4 Å (not corrected for phase shift), corresponding to the first shell, and a very broad less intense signal centered at 4 Å. The FTs of the samples at the Se K-edge are quite similar, and both the Rod 1 and Octa sample exhibit a more pronounced peak in correspondence to the first coordination shell. These results agree with the discussion on the $k^2\chi(k)$ functions at the Se K-edge, and suggest the occurrence of a structural environment with higher symmetry in the Octa sample, compatible with the sphalerite polymorph. The Se K-edge XANES spectra of the Rod 1, Octa, and pure CdSe reported in Supporting Information, Figure S7 show that Rod 1 and Octa samples have similar XANES spectra to that for CdSe, confirming that Se is tetrahedrally coordinated to Cd. However, the Octa sample has a XANES spectrum which looks slightly less like that of bulk CdSe than the XANES spectrum of the Rod 1 sample does. These differences could be consistent with the Octa sample having a sphalerite structure rather than the wurtzite structure of bulk CdSe.

On the basis of the qualitative analysis of the EXAFS and XANES data, the fitting at the Se K-edge was done using the Se−Cd and Se−Se paths calculated on the basis of the hexagonal wurtzite polymorph for the Rod 1 and Rod 2 samples, while for Octa sample two fits were performed: (i) using the Se−Cd path (one path with degeneracy 4) and Se−Se path (one path with degeneracy 12) calculated on the basis of the cubic sphalerite polymorph and (ii) using the Se−Cd and Se−Se paths calculated on the basis of the hexagonal wurtzite polymorph, as previously done for the Rod 1 and Rod 2 samples. The best fitting parameters are reported in Table 3 while the comparison of experimental vs fitting curves is reported in the Supporting Information (Figures S8 and S9). The Se−Cd distances are very similar to the values for bulk CdSe, and as expected they are longer than the Cd−S distances. The Debye−Waller factors are quite small confirming the high degree of order of the nanostructures. The fits carried out on the Octa sample, using the paths typical of the wurtzite and the paths typical of sphalerite are both quite good and provide similar results, which is not surprising since the two structures

DOI: 10.1021/acs.jpcc.5b04593
J. Phys. Chem. C 2015, 119, 16338−16348

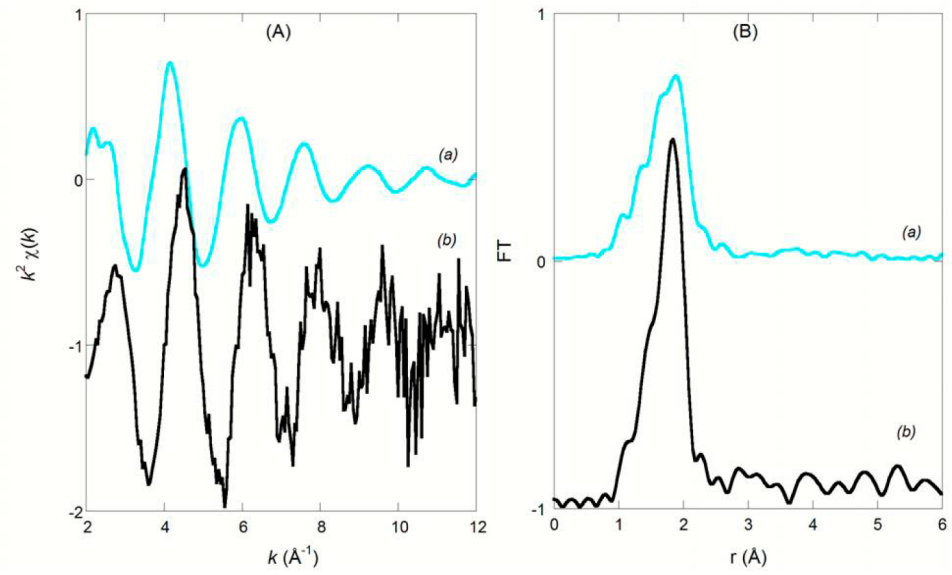

Figure 6. Experimental $k^2\chi(k)$ (A) and corresponding FTs (B) at the at the Cu K-edge for the CuCl (a) reference compound and for the Octa (b) sample.

are very similar. However, the *R*-factor of the fit carried out using the sphalerite structure is smaller, supporting that the structural environment around the Se atoms is closer to the cubic sphalerite structure.

S K-edge. EXAFS data at the S K-edge were measured on the rod, octapod, and CdS wurtzite polymorph reference compound. Data collected depositing the samples on either aluminum or sticky carbon films gave very similar results and only the experimental $k^2\chi(k)$ functions and corresponding FTs obtained for the samples deposited on the carbon sticky tape are shown in Figure 5. Although the S K-edge data are noisier with respect to the Cd and Se K-edges due to the experimental conditions required for data collection, Figure 5A clearly shows that the S K-edge $k^2\chi(k)$ of the Rod 1 and Octa samples are very similar within the experimental error and are consistent with the pure CdS wurtzite sample used as a reference. These findings are also supported by the corresponding FTs of the same samples, which show that the first shell is exactly the same and further support that in all samples the structural environment of sulfur matches with CdS in the wurtzite polymorph. Also in this case the data collected on the Rod 2 sample are very similar to the ones of the Rod 1 sample, as shown in the Supporting Information (Figure S10).

Figure S11 reporting the S K-edge XANES spectra of the Rod 1, Octa, and pure CdS samples show that Rod 1 and Octa samples have extremely similar XANES spectra to that for bulk wurtzite CdS, confirming that S is tetrahedrally coordinated to Cd.

On the basis of the qualitative insights obtained by EXAFS and XANES, the fitting at the S K-edge of experimental vs fitting curves reported in Supporting Information, Figures S12 and S13 was done using the S−Cd and S−S paths calculated on the basis of the hexagonal wurtzite polymorph for Rod 1, Rod 2 (not shown for the sake of clarity since it is also in this case very similar to sample Rod 1) and Octa samples. The best fitting parameters, reported in Table 3, are in good agreement with those obtained from the fitting at the Cd K-edge.

Cu K-Edge. On the octapod sample, the Cu K-edge was also investigated, since a copper compound is used as a starting material to induce the formation of a selenide core in the sphalerite structure, as depicted in Figure 1b. Data collected in transmission mode did not show any evidence of a Cu K-edge, which indicates the successful cation exchange of Cd(II)/Cu(I) during the synthetic protocol and that if any Cu is left, this must be below the detection limit in these experimental conditions. However, the fluorescence detector is able to provide a much more powerful tool to detect even tiny traces of an element. In fact, by using a fluorescence detector an EXAFS Cu K-edge was detected in the Octa sample. Figure 6 shows the Cu K-edge $k^2\chi(k)$ and corresponding FT which are compared to a CuCl sample used as a reference compound, having the sphalerite structure.

Although the Cu K-edge $k^2\chi(k)$ for the Octa sample is quite noisy, as expected due to the very low Cu content, oscillations are evident up to at least k = 10 Å^{-1} and therefore some structural information can be inferred. In particular, the comparison of the $k^2\chi(k)$ and the FT of the octapods with those of the CuCl compound in the sphalerite polymorph shows that the oscillations in the $k^2\chi(k)$ are significantly shifted, indicating that the copper environment in the Octa sample is not the same as in CuCl. In particular, the significant shift in the oscillations is consistent with the Cu environment, having a much heavier backscatterer, such as Se, compared to Cl. The amplitude of the oscillations and the magnitude of the FT peak is higher in the Octa sample compared with the CuCl, which also indicates that a heavier backscatterer must be present. Nevertheless, the frequency of the oscillation is similar, and the main peak in the FTs of CuCl and the Octa sample is centered at approximately the same distance. This is understandable, considering that the Cu−Cl distance in the first coordination shell of CuCl and the Cu−Se distance in the first shell of $Cu_{2-x}Se$ (this compound, berzelianite, having a cubic structure belonging to space group *Fm*3*m*) are similar. The observed results are consistent with the presence of a tiny amount of copper in CdSe.

It is interesting to note that the availability of a high intensity EXAFS beamline with a very sensitive fluorescence detector is able to evidence very small amounts of precursors which have

DOI: 10.1021/acs.jpcc.5b04593
J. Phys. Chem. C 2015, 119, 16338−16348

not completely reacted. The role of EXAFS in gaining insights on multicomponent materials, even on trace elements which are not detected by other structural techniques, is also confirmed by the fact that, while collecting data on the octapods at the Cu K-edge in transmission mode in an extended energy range, a very small but well-defined edge at 9659 eV corresponding to the Zn K-edge was detected (see Supporting Information, Figure S14) even if, as previously pointed out, no evidence of the presence of Cu was found. The Zn edge is not visible in fluorescence mode since Zn cannot be excited at the energy of Cu K-edge. The occurrence of Zn in these samples, although in low amount, was unexpected since all reagents were of high purity. The most likely source of this impurity is a Zn impurity in one of the Cd reagents, since Cd is the element present in largest amount. These results point out the importance of controlling the presence of undesired metal traces, which may affect to some extent the physical properties of the resulting nanocrystals.

4. CONCLUSIONS

CdSe@CdS heterostructures prepared by high temperature colloidal routes with a highly controlled morphology, that is, nearly monodisperse elongated dot@rods and branched dot@octapods, were studied by multiedge X-ray absorption spectroscopy investigation.

In particular, dot@rods samples with the same diameter (6 nm) and different length (from around 20 to 30 nm) and a dot@octapod sample were investigated at the Cd, S, and Se K-edges to gain insights on the local structure by taking advantage of the selectivity of X-ray absorption spectroscopy. On the basis of the comparison of the EXAFS and XANES spectra of the samples with the reference bulk structures (CdS and CdSe wurtzite polymorphs), a quantitative analysis of the EXAFS data was performed to evaluate distances, coordination numbers, and Debye−Waller factors.

In the case of CdSe@CdS dot@rods, which are prepared through a well-established procedure, all the data indicate the occurrence of a CdSe core and a CdS rod both in the wurtzite polymorph. The structural features are identical regardless of the size of the rods, and comparison with the corresponding pure reference compound, that is, CdSe and CdS wurtzite polymorphs, points out the high crystallinity of the core and of the rod. This result supports the effectiveness of high temperature colloidal synthesis in promoting the formation of core@shell nanocrystals with very low defectivity.

In the case of CdSe@CdS dot@octapods, EXAFS at the Se K-edge provided insights on the CdSe core, indicating the occurrence of a structural environment with high symmetry compatible with the CdSe sphalerite cubic polymorph. It was also found that the structure of the octapod arms is the same encountered in the rods and is the same as pure CdS wurtzite reference compound. In addition the Cd, S, and Se K-edge XANES spectra supported all of the above conclusions, providing evidence of the presence of the CdSe sphalerite core, which cannot be assessed by XRD and UV−visible spectroscopy characterization, in the final CdSe@CdS dot@octapods.[27]

Measurements at the Cu K-edge on the Octa sample allowed us to point out the occurrence of traces of copper having a structural environment in which copper has Se nearest neighbors, suggesting the occurrence of Cu in the octapods. Although the detailed location of the Cu ions cannot be directly determined without the support of electron microscopy techniques, indirect evidence is gained by the nature of the backscatterers surrounding the Cu atoms, which suggests that Cu is likely present in the CdSe sphalerite seed. The high sensitivity and selectivity of the EXAFS technique enabled therefore the detection of the traces of the copper selenide phase which is formed in situ and used to produce the CdSe sphalerite dots upon cation exchange. These findings represent the first experimental support in agreement with the proposed model used for CdSe@CdS octapod design and synthesis. In addition, elucidation of the structural features of the investigated heterostructures may provide a basis for the interpretation of their optical properties.

Despite the intrinsic limitation of X-ray absorption techniques due to the limited access to synchrotron light facilities and to the requirement of constituent nanocrystals with extremely controlled size and shape distribution, our study points out the relevance of advanced structural investigation techniques such as EXAFS in revealing the structural features of multicomponent nanostructures, which in turn play a key role in the design of heterostructures with controlled architectures and in establishing well-defined synthesis−structure-properties relationships for such materials.

■ ASSOCIATED CONTENT

Ⓢ Supporting Information

Comparison of the data at the Cd, Se and S K-edge for the Rod 1 and Rod 2 samples; XANES spectra at the at the Cd, Se, and S K-edge; differences at the Cd K-edge between the EXAFS of Rod 1, Octa, and CdSe with respect to CdS; Fit results at the Cd, Se and S K-edge for the Rod 1 and Octa samples; EXAFS spectrum at the Cu K edge for the Octa sample. The Supporting Information is available free of charge on the ACS Publications website at DOI: 10.1021/acs.jpcc.5b04593.

■ AUTHOR INFORMATION

Corresponding Authors

*E-mail: a.corrias@kent.ac.uk.
*E-mail: casulaf@unica.it.

Notes

The authors declare no competing financial interest.

■ ACKNOWLEDGMENTS

This work has been supported by the Regione Autonoma della Sardegna under Project CRP18013-2009 L.R. 7/2007. We also thank Diamond Light Source for access to beamline B18 (Proposal SP9759) that contributed to the results presented here. Dr. Andrea Falqui and Mee-Rahn Kim are gratefully acknowledged for their support at early stages of this project.

■ REFERENCES

(1) Kudera, S.; Carbone, L.; Manna, L.; Parak, W. J. *Growth Mechanism, Shape and Composition Control of Semiconductor Nanocrystals, in Semiconductor Nanocrystal Quantum Dots*; Rogach, A. L., Ed.; Springer: Wien, Germany, 2008.

(2) Li, H.; Kanaras, A. G.; Manna, L. Colloidal Branched Semiconductor Nanocrystals: State of the Art and Perspectives. *Acc. Chem. Res.* **2013**, *46*, 1387−1396.

(3) Kovalenko, M. V.; Manna, L.; Cabot, A.; Hens, Z.; Talapin, D. V.; Kagan, C. R.; Klimov, V. I.; Rogach, A. L.; Reiss, P.; Milliron, D. J.; et al. Prospects of Nanoscience with Nanocrystals. *ACS Nano* **2015**, *9*, 1012−1057.

(4) Saruyama, M.; So, Y.-G.; Kimoto, K.; Taguchi, S.; Kanemitsu, Y.; Teranishi, T. Spontaneous Formation of Wurzite-CdS/Zinc Blende-

DOI: 10.1021/acs.jpcc.5b04593
J. Phys. Chem. C 2015, 119, 16338−16348

CdTe Heterodimers through a Partial Anion Exchange Reaction. *J. Am. Chem. Soc.* **2011**, *133*, 17598−17601.
(5) Zhang, D.; Wong, A. B.; Yu, Y.; Brittman, S.; Sun, J.; Fu, A.; Beberwyck, B.; Alivisatos, A. P.; Yang, P. Phase Selective Cation-Exchange Chemistry in Sulfide Nanowire Systems. *J. Am. Chem. Soc.* **2014**, *136*, 17430−17433.
(6) Carbone, L.; Nobile, C.; DeGiorgi, M.; DellaSala, F.; Morello, G.; Pompa, P.; Hytch, M.; Snoeck, E.; Fiore, A.; Franchini, I. R.; et al. Synthesis and Micrometer-Scale Assembly of Colloidal CdSe/CdS Nanorods Prepared by a Seeded Growth Approach. *Nano Lett.* **2007**, *7* (10), 2942−2950.
(7) Talapin, D. V.; Nelson, J. H.; Shevchenko, E. V.; Aloni, S.; Sadtler, B.; Alivisatos, A. P. Seeded Growth of Highly Luminescent CdSe/CdS Nanoheterostructures with Rod and Tetrapod Morphologies. *Nano Lett.* **2007**, *7*, 2951−2959.
(8) Luo, Y.; Wang, L. W. Electronic Structures of CdSe/CdS Core Shell Nanorods. *ACS Nano* **2010**, *4*, 91−98.
(9) Brescia, R.; Miszta, K.; Dorfs, D.; Manna, L.; Bertoni, G. Birth and Growth of Octapod-Shaped Colloidal Nanocrystals Studied by Electron Tomography. *J. Phys. Chem. C* **2011**, *115*, 20128−20133.
(10) Corrado, C.; Jiang, Y.; Oba, F.; Kozina, M.; Bridges, F.; Zhang, J. Z. Synthesis, Optical and Structural Properties of Cu-doped ZnS Nanomaterials. *J. Phys. Chem. A* **2009**, *113*, 3830−3839.
(11) Sakamoto, M.; Inoue, K.; Saruyama, M.; So, Y.-G.; Kimoto, K.; Okano, M.; Kanemitsu, Y.; Teranishi, T. Investigation on Photo-induced Charge Separation in CdS/CdTe Nanopencils. *Chem. Sci.* **2014**, *5*, 3831−3835.
(12) Koninbsberger, D. C.; Prins, R. *X-Ray Absorption: Principles, Applications, Techniques of EXAFS*, SEXAFS and XANES Eds; Wiley: New York, 1987.
(13) Bordiga, S.; Groppo, E.; Agostini, G.; Van Bokhoven, J. A.; Lamberti, C. Reactivity of Surface Species in Heterogeneous Catalysts Probed by In Situ X-Ray Absorption Techniques. *Chem. Rev.* **2013**, *113*, 1736−1850.
(14) Mostafa, S.; Behafarid, F.; Croy, J. R.; Ono, L. K.; Li, L.; Yang, J. C.; Frenkel, A. I.; Cuenya, B. R. Shape-Dependent Catalytic Properties of Pt Nanoparticles. *J. Am. Chem. Soc.* **2010**, *132*, 15714−15719.
(15) Mandal, S.; Mandale, A. B.; Sastry, M. Keggin Ion-Mediated Synthesis of Aqueous Phase-pure Au@Pd and Au@Pt Core-Shell Nanoparticles. *J. Mater. Chem.* **2004**, *14*, 2868−2871.
(16) Carta, D.; Mountjoy, G.; Gass, M.; Navarra, G.; Casula, M. F.; Corrias, A. Structural Characterisation Study of FeCo Alloy Nanoparticles in a Highly Porous Aerogel Silica Matrix. *J. Chem. Phys.* **2007**, *127*, 204705.
(17) Padovani, S.; Sada, C.; Mazzoldi, P.; Brunetti, B.; Borgia, I.; Sgamellotti, A.; Giulivi, A.; D'Acapito, F.; Battaglin, G. Copper in Glazes of Renaissance Luster Pottery: Nanoparticles, Ions, and Local Environment. *J. Appl. Phys.* **2003**, *93*, 10058−10063.
(18) Carta, D.; Mountjoy, G.; Navarra, G.; Casula, M. F.; Loche, D.; Marras, S.; Corrias, A. X-Ray Absorption Investigation of the Formation of Cobalt Ferrite Nanoparticles in an Aerogel Silica Matrix. *J. Phys. Chem. C* **2007**, *111*, 6308−6317.
(19) Carta, D.; Casula, M. F.; Mountjoy, G.; Corrias, A. Formation and Cation Distribution in Supported Manganese Ferrite Nanoparticles: an X-Ray Absorption Study. *Phys. Chem. Chem. Phys.* **2008**, *10*, 3108−3117.
(20) Carta, D.; Loche, D.; Mountjoy, G.; Navarra, G.; Corrias, A. $NiFe_2O_4$ Nanoparticles Dispersed in an Aerogel Silica Matrix: An X-Ray Absorption Study. *J. Phys. Chem. C* **2008**, *112*, 15623−15630.
(21) Carta, D.; Casula, M. F.; Falqui, A.; Loche, D.; Mountjoy, G.; Sangregorio, C.; Corrias, A. A Structural and Magnetic Investigation of the Inversion Degree in Ferrite Nanocrystals MFe_2O_4 (M = Mn, Co, Ni). *J. Phys. Chem. C* **2009**, *113*, 8606−8615.
(22) Carta, D.; Corrias, A.; Falqui, A.; Brescia, R.; Fantechi, E.; Pineider, F.; Sangregorio, C. EDS, HRTEM/STEM, and X-Ray Absorption Spectroscopy Studies of Co-Substituted Maghemite Nanoparticles. *J. Phys. Chem. C* **2013**, *117*, 9496−9506.
(23) Carta, D.; Marras, C.; Loche, D.; Mountjoy, G.; Ahmed, S. I.; Corrias, A. An X-Ray Absorption Spectroscopy Study of the Inversion Degree in Zinc Ferrite Nanocrystals Dispersed on a Highly Porous Silica Aerogel Matrix. *J. Chem. Phys.* **2013**, *138*, 054702.
(24) Rockenberger, J.; Troger, L.; Rogach, A. L.; Tischer, M.; Grundmann, M.; Eychmuller, A.; Weller, H. *J. Chem. Phys.* **1998**, *108*, 7807−7815.
(25) Marcus, M. A.; Flood, W.; Stiegerwald, M.; Brus, L.; Bawendi, M. Structure of Capped Cadmium Selenide Clusters by EXAFS. *J. Phys. Chem.* **1991**, *95*, 1572−1576.
(26) Kim, M. R.; Miszta, K.; Povia, M.; Brescia, R.; Christodoulou, S.; Prato, M.; Marras, S.; Manna, L. The Influence of Chloride Ions on the Synthesis of Colloidal Branched CdSe/CdS Nanocrystal by Seeded Growth. *ACS Nano* **2012**, *6*, 11088−11096.
(27) Conca, E.; Aresti, M.; Saba, M.; Casula, M. F.; Quochi, F.; Mula, G.; Loche, D.; Kim, M. R.; Manna, L.; Corrias, A.; et al. Pt Decoration of CdSe@CdS Octapods: Effects on Charge Separation. *Nanoscale* **2014**, *6*, 2238−2243.
(28) Klug, H. P.; Alexander, L. E. *X-Ray Diffraction Procedures*; Wiley: New York,1974.
(29) Dent, A. J.; Cibin, G.; Ramos, S.; Smith, A. D.; Scott, S. M.; Varandas, L.; Pearson, M. R.; Krumpa, N. A.; Jones, C. P.; Robbins, P. E. *J. Phys. Conf. Ser.* **2009**, *190*, 012039.
(30) Ravel, B.; Newville, M. ATHENA, ARTEMIS, HEPHAESTUS: Data Analysis for X-Ray Absorption Spectroscopy Using IFEFFIT. *J. Synchrotron Radiat.* **2005**, *12*, 537−541.
(31) Deka, S.; Miszta, K.; Dorfs, D.; Genovese, A.; Bertoni, G.; Manna, L. Octapod-Shaped Colloidal Nanocrystals of Cadmium Chalcogenides via "One-Pot" Cation Exchange and Seeded Growth. *Nano Lett.* **2010**, *10*, 3770−3776.
(32) Greegor, R. B.; Lytle, F. W. Morphology of Supported Metal Clusters: Determination by EXAFS and Chemisorption. *J. Catal.* **1980**, *63*, 476−486.

DOI: 10.1021/acs.jpcc.5b04593
J. Phys. Chem. C 2015, 119, 16338−16348